

Nonlinear Optical Properties of *meso*-Tetra(fluorenyl)porphyrins Peripherally Functionalized with One to Four Ruthenium Alkynyl Substituents

Xu Zhang,^a Limiao Shi,^a Mark A. Fox,^b Adam Barlow,^c Mahbod Morshedi,^c Marie P. Cifuentes,^c Mark G. Humphrey,^{c,*} Olivier Mongin,^a Frédéric Paul,^{a,*} and Christine O. Paul-Roth^{a,*}

- ^{a.} Univ Rennes, INSA Rennes, CNRS, ISCR (Institut des Sciences Chimiques de Rennes) – UMR 6226, F-35000 Rennes, France.
^{b.} Department of Chemistry, Durham University, Durham, DH1 3LE, U.K.
^{c.} Research School of Chemistry, Australian National University, Canberra ACT 2601, Australia.

Electronic Supplementary Information (ESI) available: Synthesis of the aldehyde **11**, NMR spectra, cyclic voltammograms, emission spectra and Z-scan data for selected compounds.

ABSTRACT

The synthesis of a series of four porphyrin derivatives based on a *meso*-tetrafluorenylporphyrin core functionalized with one to four *trans*-chlorobis(dppe)ruthenium alkynyl units (dppe = 1,2-bis(diphenylphosphino)ethane) at the periphery, together with cyclic voltammetry (CV) and UV-vis absorption and emission spectroscopy studies, are reported. In these multipolar assemblies, the organoruthenium endgroups are potential electron-donors and the central porphyrin core is a potential electron-acceptor. The third-order nonlinear optical (NLO) responses have been assessed by Z-scan, revealing that these extended π -networks incorporating polarizable organometallic units behave as nonlinear absorbers in the near-IR range. The role of the peripheral transition metal centers on the third-order NLO properties is discussed.

Keywords

Porphyrin • Fluorenyl • Ruthenium • UV-Vis Absorption • Nonlinear absorption

1. Introduction

Recently, there has been an increasing interest in multi-photon absorbing molecules and materials, driven by the upsurge in key societal applications that can exploit these substances,¹ namely photonic devices for laser beam control,² optical data storage,³ microfabrication,⁴ fluorescence imaging, and photodynamic therapy.⁵

Among the panoply of possibilities, certain organometallic compounds^{6, 7} such as group 8 transition metal alkynyl complexes stand out as attractive building blocks because their nonlinear optical (NLO) properties are often significantly larger than those of purely organic analogues.⁸ Thus, many examples of formally octahedral d⁶ complexes featuring an equatorial Ru(dppe)₂ core [dppe = 1,2-bis(diphenylphosphino)ethane] have been explored.⁹ When incorporated into extended π networks, a remarkable enhancement of the NLO responses is

often observed.^{10, 11} In the pursuit of optimized systems, these organometallic units permit great structural control, as the ligand *trans* to the alkynyl ligand can be varied at will, affording the possibility of fine-tuning their NLO performance. In parallel work, large metallated π -compounds such as porphyrins or phthalocyanines have also been identified as promising cubic NLO-phores.¹²⁻¹⁴ For instance, Rao *et al.* showed that various metallated *meso*-tetra(*p*-tolyl)porphyrins (TTP) exhibit high cubic optical nonlinearities at 532 and 600 nm.¹⁵ Thus, depending on the overall symmetry of the tetrapyrrolic core, on the nature of the central metal ion (if any), and on the nature of the peripheral substituents appended to the macrocyclic core, widely different nonlinearities can result. To achieve high hyperpolarizabilities, the presence of a metal inside the porphyrin cavity is usually recommended, since, besides electronic effects, it facilitates planarization of the macrocyclic π -manifold.^{13, 14}

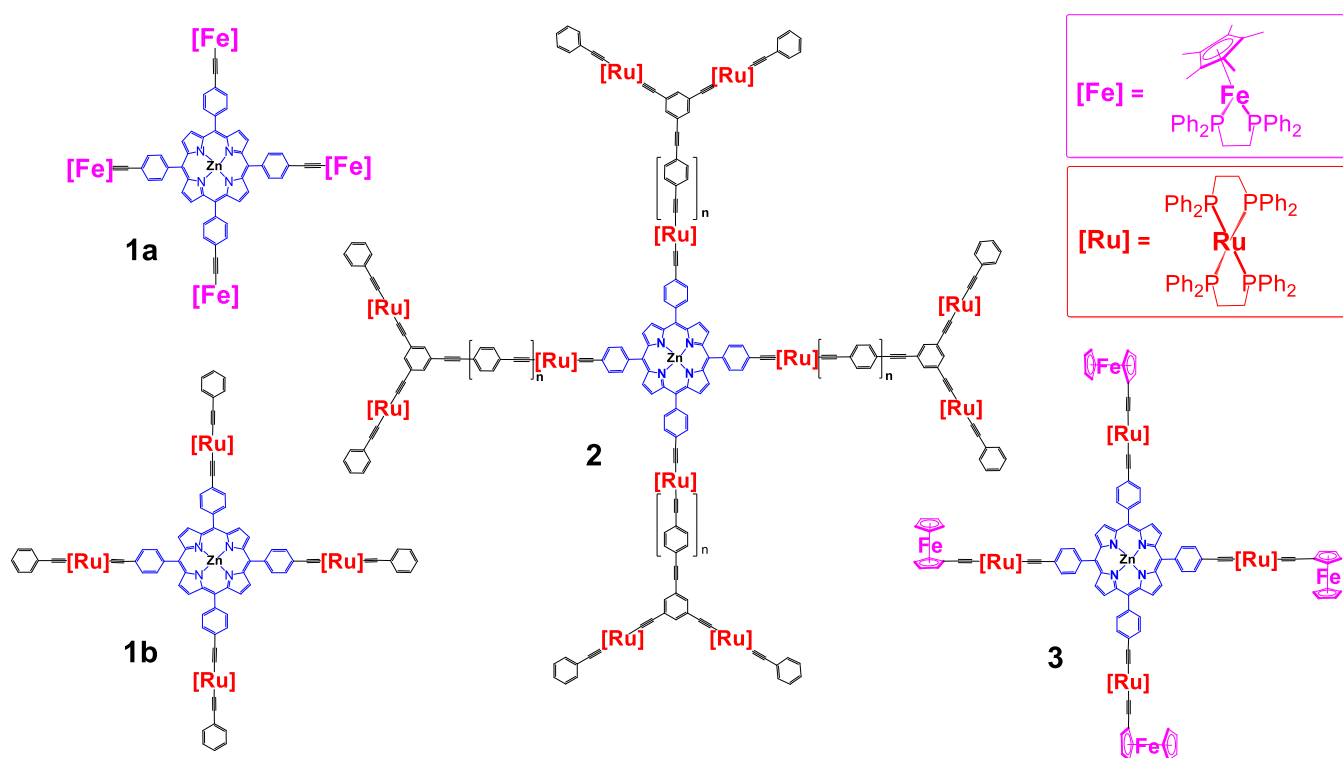


Figure 1. ZnTPP-based polymetallated tetragonal arrays with strong near-IR nonlinear absorption.

Based on these observations, some of us showed in 2012 that zinc(II) *meso*-tetraphenylporphyrins (ZnTPPs), *p*-phenyl-substituted by four Fe(II)¹⁶ or Ru(II)¹⁷ alkynyl moieties (**1a-1b**; Figure 1), can possess strong nonlinear absorption properties

in the near-IR region. More recently, and taking advantage of the coordination site available on the peripheral Ru(II) atoms, the π -manifold was expanded by either Ru(II)-containing dendrons (**2**)¹⁸ or organoiron-alkynyls (**3**).^{16, 19} Larger third-

order NLO responses and significant nonlinear absorption in the near-IR were seen for both **2** and **3**, as exemplified by the impressive values found for the maximal “effective” two-photon absorption cross-sections (σ_2) in this spectral range.²⁰ However, no general explanation correlating the electronic structures of these macrocycles to these phenomena has been presented so far. It was the goal of the present contribution to attempt to rationalize the unusual nonlinear absorption observed in the near-IR for such oligo(metal-alkynyl)porphyrins.^{21, 22} To achieve this, we have pursued

analogues of **5a**, namely **5b** and **5c**, as well as the fully symmetric **5d** (Figure 2B). The free-base *meso*-tetra(fluorenyl)porphyrin (H₂TFP) derivatives **4** and **5a** (Figure 2A) had previously been targeted for spectrofluorochromic investigations.^{23, 24} However, the redox-triggered fluorochromic contrast was weak for both compounds because the fluorescence of the H₂TFP core²⁵ is efficiently trapped in both the Ru(II) and Ru(III) redox states.^{24, 26}

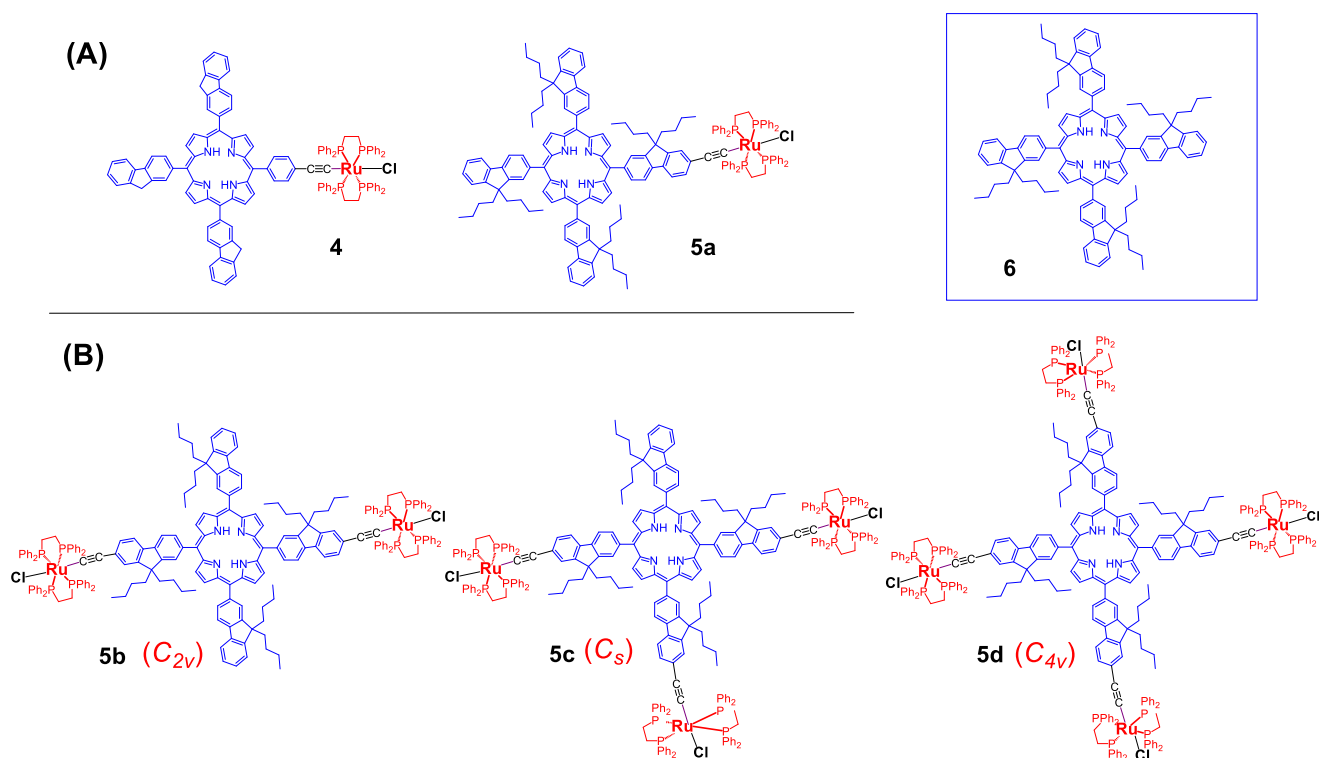


Figure 2. Selected free-base *meso*-tetra(aryl)porphyrins. Known derivatives previously used for redox-modulation of fluorescence (**4** and **5a**: **A**), new compounds targeted for this work (**5b-5d**: **B**) and the free-base porphyrin used to model the properties of the core (**6**: inset).

We have now isolated the di-, tri- and tetra-metallated analogues of **5a** and report the third-order NLO properties of the full series **5a-d** (Figure 2). These organometallic tetra(fluorenyl)porphyrins permit assessment of the effect of stepwise incorporation of metal alkynyl substituents at the periphery on the 2PA properties. Functionalization of the fluorenyl units by *n*-butyl groups enhances solubility in organic solvents, a key requirement for Z-scan studies. We expected the expanded π -manifold on the arms to increase the third-order NLO response compared to porphyrins such as **1a-b** previously studied. In addition, the lower symmetry of the peripheral arms in **5b** and **5d**¹ and of the free-base core should

reduce the contribution of centrosymmetric conformers for which the exclusion rule holds.^{1, 27} This should in turn facilitate comparison of the one- and two-photon spectra (1PA and 2PA, respectively) for all in this series and therefore also facilitate identification of relevant excited states responsible for multi-photon absorption (MPA). Finally, the organic porphyrin **6** is included as a model for the 1PA properties of the core.²⁸ The latter can be isolated following well established synthetic approaches.^{28, 29} We therefore herein report (i) the synthesis and characterization of the new derivatives **5b-5d** and (ii) the linear and nonlinear (third-order) optical properties of **5a-5d**.

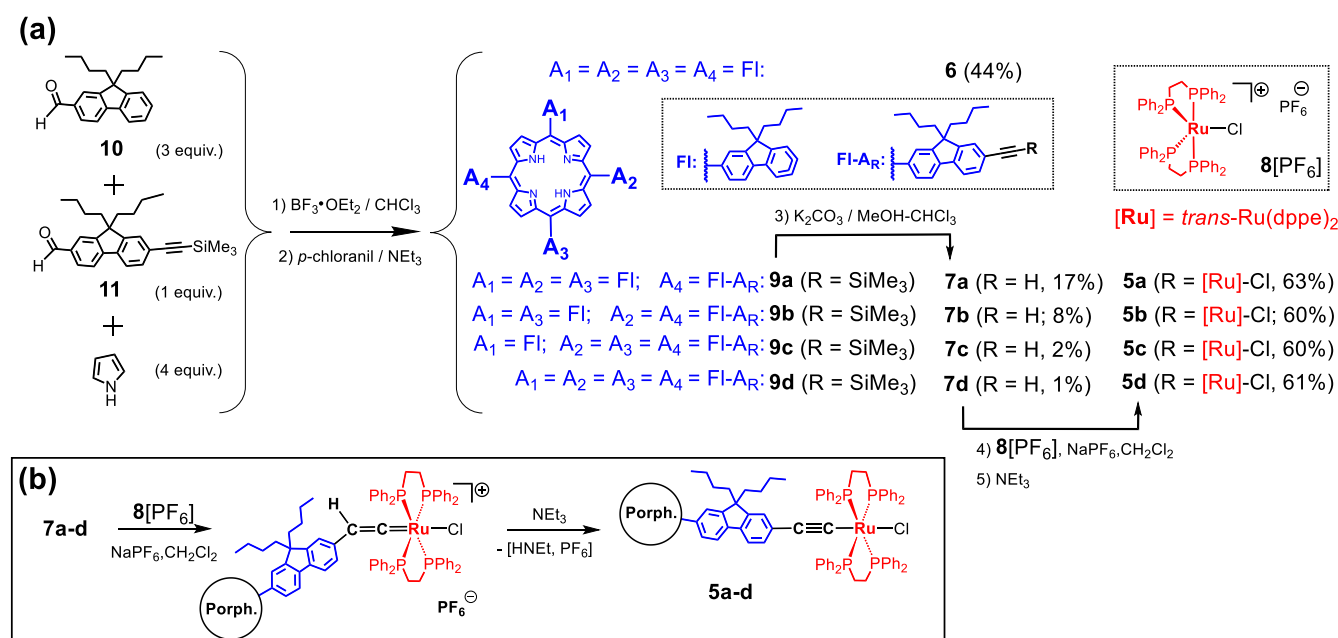
¹ **5b** and **5d** have a centre of symmetry, whereas **5a** and **5c** do not, and so only the former should be subject to the exclusion rule.

2. Results and discussion

Synthesis

To obtain the targeted mono-, di-, tri- and tetra-ruthenium derivatives (**5a-5d**) shown in Figure 2, the corresponding alkyne precursors **7a-7d** were first prepared. These A₃B, A₂B₂, AB₃ and B₄ organic porphyrins were obtained from trimethylsilyl-protected precursors (**9a-9d**), themselves isolated from a porphyrin-reaction mixture of the aldehydes **10**³⁰ and **11**.^{31, 32} Thus, **10** and **11**³² were reacted in a 3:1 ratio under Lindsey conditions³³ to favour the formation of **9a-9b** over **9c-9d**, with **9d** being subsequently accessed from **11**.³⁴ The porphyrin **9a** is important for comparison purposes since it provides access to **5a** which allows us to model the effect of one metallated branch on the optical properties. Separation of the various porphyrins was not possible on silica gel, presumably because of the very similar polarities of **6** and **9a-9d**, so the mixture of compounds as a dark red solid fraction

was used directly in the next step *viz.* desilylation of the alkynes. The cleavage of the trimethylsilyl (TMS) groups was achieved by using an excess of K₂CO₃ and heating at 60 °C. Purification of the porphyrin components **6** and **7a-7d** was effected on silica gel by sequential chromatographic separations. The yield of **7d** is low, the reaction of necessity being repeated from **11** to obtain sufficient quantities (the isolated yield of **7d** from **11** is 28%).³⁴ Only one (the *trans* isomer, **7b**) of the two possible isomers of the bis(terminal alkyne) derivative was isolated. The pendant alkynes of **7a-7d** were then metallated using the corresponding amounts of the ruthenium(II) salt **8**[PF₆] (Scheme 1).³⁵ In each case, the reaction was followed by ³¹P and ¹H NMR spectroscopies to ensure the starting material was fully consumed (> 72 h). The complex **8**[PF₆] is characterized by two diagnostic triplets at 55.8 and 83.7 ppm (³¹P), successful reaction being confirmed by disappearance of these resonances and the diagnostic singlets at ca. 3.2 ppm (¹H NMR) of the terminal alkynes **7b-7d**.



Scheme 1. (a) Synthesis of **6**, alkyne precursors **7a-7d**, and organometallic derivatives **5a-5d**. (b) The inset shows the structure of the (poly)vinylidene intermediates formed in the medium at step 4).

At this stage, the vinylidene intermediates which have formed (characterized by singlets at ca. 37 ppm in the ³¹P NMR spectra) were deprotonated *in situ* by NEt₃ to give the desired organometallic complexes (Scheme 1b).² The reaction mixtures were then quickly passed through basic alumina to remove any traces of unreacted **8**[PF₆] or polar impurities resulting from vinylidene decomposition. Yields of ca. 60% of the metallated porphyrins were obtained in each case. The new organic porphyrins **7b-7d** and the corresponding organometallic

porphyrins **5b-5d** were then characterized by NMR (CDCl₃), HRMS and elemental analyses.

NMR data

Organic derivatives 6 and 7a-7d. Partial ¹H NMR spectra of **7a-7d** are compared to that of the reference compound **6** in Figure 3a. Characteristic signals are obtained for all protons in four spectral ranges: (i) Eight β-pyrrolic H around 9 ppm and two NH protons around -3 ppm, (ii) 25 to 28 fluorenyl aromatic protons between 8 and 6 ppm, (iii) 1 to 4 H alkyne proton(s) at ca. 3 ppm and (iv) 64 aliphatic protons for the *n*-butyl chains appearing as a set of four signals at 0-3 ppm (whether or not

² Compounds **5a-5d** have nearly the same solubility as their free-base porphyrin precursors **7b-7d**, so purification by selective precipitation cannot be conveniently used.

the fluorenyl groups are equivalent). The β -pyrrolic protons shift slightly to higher field, from 8.93 to 8.90, upon stepwise alkylation of the *meso*-fluorenyl groups. The perfectly symmetrical AB signal observed for the single isomer of **7b** (in the frame) suggests that the two alkyne units are located on *trans*-fluorenes rather than on *cis*-disposed fluorenes (for which one doublet and two distinct singlets in a 2:1:1 ratio would be expected). In the aromatic region, the signals

attributed to H_{5-8} and $H_{5'-8'}$ are also particularly sensitive to the alkylation of the fluorene, with the $H_5:H_{5'}$ ratio corresponding to the ratio of the different fluorene groups in each molecule (in this respect, the aliphatic and NH signals are far less reliable markers).

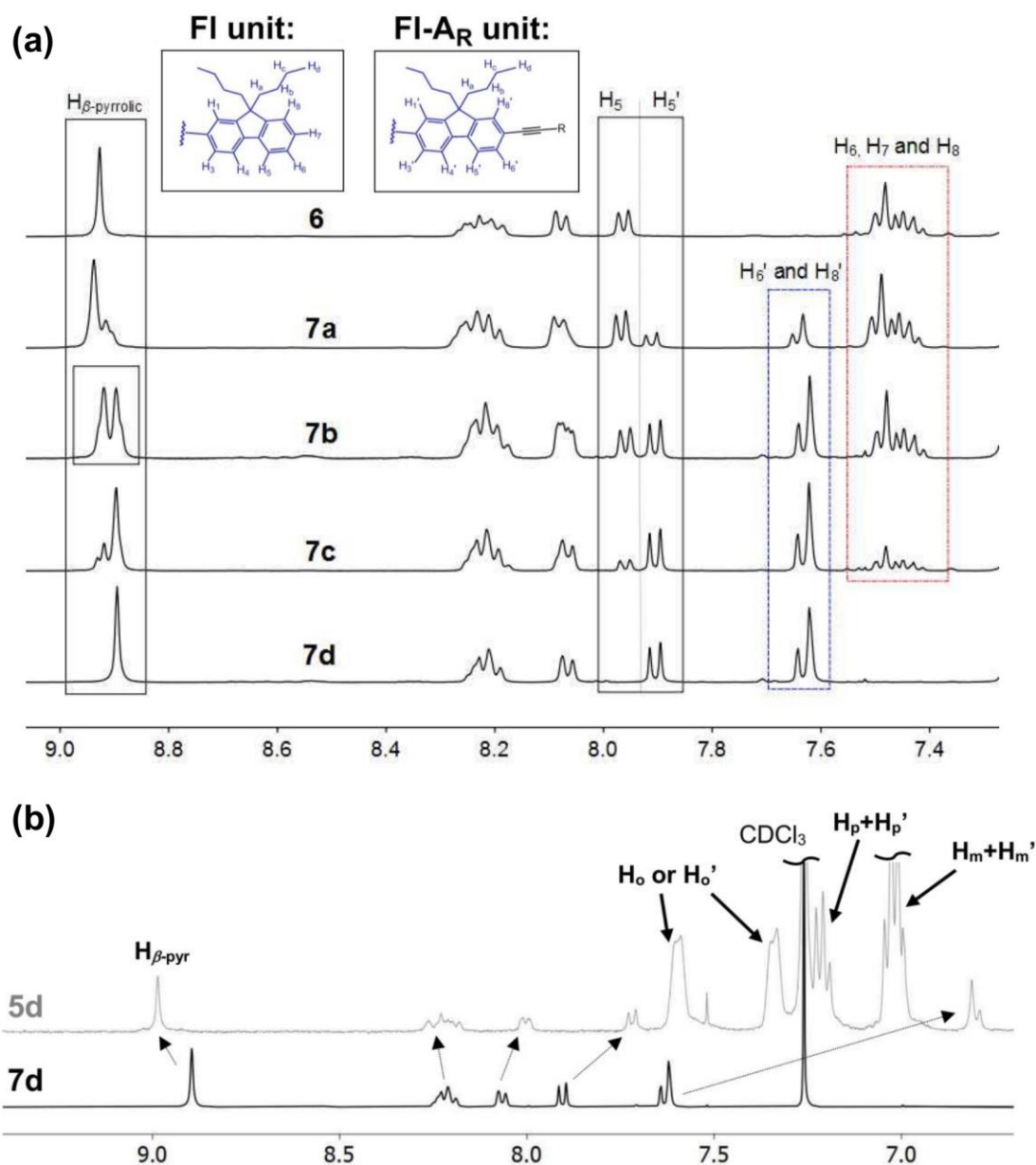


Figure 3. (a) Comparison of the ^1H NMR spectra of **6** and **7a-7d** in the aromatic range. (b) Comparison between **5d** and **7d** in the aromatic range. The additional aromatic dppe protons (see ESI for details) in **5d** and the shifts of selected TFP protons are indicated.

Organometallic derivatives 5a-5d. By comparison, the ^1H NMR spectra of the ruthenium derivatives **5a-5d** clearly reveal the presence of four additional signals in the aromatic range (H_0 , $H_{0'}$, $H_{m+m'}$ and $H_{p+p'}$: see Figure 3b and ESI) which are indicative of the presence of the dppe phenyl protons. In addition, a

multiplet near 2.8 ppm, diagnostic of methylene protons, further confirms the presence of the dppe-containing co-ligands. When progressing from **5a** to **5d**, the intensity of these signals increases in a stepwise way with the increasing number of ruthenium substituents. Interestingly, for **5b**, the eight β -

pyrrolic protons now appear as two overlapped doublets, around 9.0 ppm, confirming the *trans*-assignment of the isolated isomer, consistent with the corresponding symmetry assumed for **7b**. In addition, the presence of the organometallic end-groups in **5a-5d** is confirmed by diagnostic singlets in the ^{31}P NMR (Table 1), around 49 ppm, which correspond to the four, eight, twelve and sixteen equivalent phosphorus nuclei of the dppe ligands. Similar NMR signatures have previously been observed for the related organometallic compounds **12**¹⁷ and **13**³⁶ (Figure 4).

Table 1. Characteristic ^{31}P NMR and cyclic voltammetric data for organometallic porphyrins **5a-5d** and reference compounds **6**, **12**, and **13**.

| Cmpd | $^{31}\text{P}\{^1\text{H}\}$ NMR (ppm) ^a | E° (V vs SCE) ^b | | |
|------------------------|--|-----------------------------------|--------------------------------------|---------------------------------------|
| | | [Ru(III/II)] E° | [Porphyrin] E°_{Ox} | [Porphyrin] E°_{Red} |
| 5a ^c | 49.4 | 0.42 | 0.99, 1.33 | -1.21 |
| 5b | 49.4 | 0.42 | 0.99, 1.33 | -1.20 |
| 5c | 49.5 | 0.43 | 1.00, 1.35 | -1.21 |
| 5d | 49.5 | 0.43 | 1.03, 1.36 | -1.25 |
| 6 | / | / | 0.99, 1.38, 1.70 | -1.14 -1.50 |
| 12 ^d | 51.0 | 0.49 | 0.87, 1.16 | / |
| 13 ^e | 50.2 | 0.41 | / | / |

^a CDCl_3 , ^b CH_2Cl_2 , 20 °C, 0.1 M $[\text{NBu}_4][\text{PF}_6]$, scan rate 0.1 V.s⁻¹ with ferrocene or decamethylferrocene used as internal calibrants. Potentials are expressed relative to that of the saturated calomel electrode (SCE), with the $\text{Cp}^*_2\text{Fe}^+/\text{Cp}^*_2\text{Fe}$ couple at -0.08 V (see Exp. Part).³⁷ ^c Data from ref. ²⁴, ^d Data from ref. ¹⁷, ^e Data from ref. ³⁶.

Cyclic voltammetry measurements

Cyclic voltammetry (CV) studies of the porphyrins **5a-5d** and **6** were carried out in dichloromethane, with $[\text{NBu}_4][\text{PF}_6]$ (0.1 M) as supporting electrolyte (Table 1). In line with published data for **5a**²⁴ and the related molecules **1b** and **12**,¹⁷ the organometallic compounds **5b-5d** show the classic ring-centered oxidations and reduction of the H_2TFP free-base porphyrin, as modelled by **6**, plus a Ru-centered oxidation at ca. 0.42 V, at nearly the same potential as that measured for the 2-fluorenylalkynyl Ru(II) complex **13**³⁶ and close to that for the Ru-centered oxidation of **12**²⁴ (Table 1).

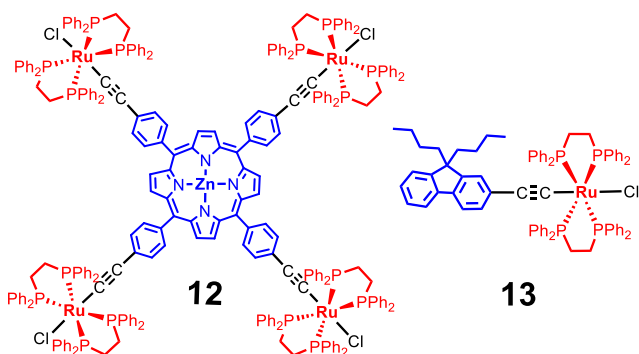


Figure 4. Selected compounds related to **5a-5d**.

Upon progressing from **5a** to **5d**, the intensity of this redox process increases relative to the porphyrin-based processes, consistent with the increasing number of ruthenium atoms in the molecule (Figure S11, ESI). Only one redox wave is observed in the oligo-ruthenated compounds **5b-5d**. This results from the overlap of two to four one-electron redox waves corresponding to the oxidation/reduction of each Ru(II) endgroup (Figure 5), in line with a weak through-porphyrin electronic communication between the redox-active organometallic units in these compounds.²¹ Similar to previous observations with **1b**, **2**, and **3**,^{17, 19, 20} the chemical reversibility of these (Ru(II)-centered) oxidations and their potential difference with the first porphyrin-based oxidation (≥ 570 mV) opens the possibility of using them for switching the NLO properties of **5a-5d**.⁸

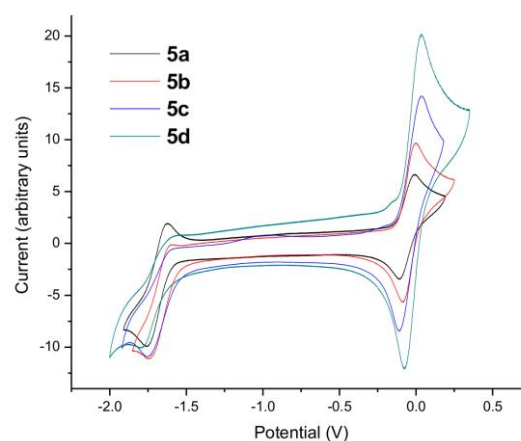


Figure 5. Cyclic voltammograms for **5a-d** (vs. the $\text{Cp}_2\text{Fe}^+/\text{Cp}_2\text{Fe}$) redox couple used as reference and set at 0.0 V.

DFT computations

Geometry optimizations of models of **5b-5d**, where the butyl groups were replaced with hydrogens (denoted as **5b'-5d'**), were carried out using the hybrid DFT functional B3LYP with the 3-21G* basis set for all atoms. B3LYP/3-21G* has been shown to be suitable to model alkynyl ruthenium complexes elsewhere³⁸ and this level of theory was previously used to successfully model **5a** (as **5a'**). Because the butyl groups in **5b-5d** do not contribute significantly to the important frontier orbitals, they were replaced with hydrogens (affording the models **5b'-5d'**), which reduces the computational expense for these large molecules during geometry optimizations (this replacement was previously carried out successfully with **5a/5a'**).²⁴ Under these conditions, the Ru...Ru and Cl...Cl distances in **5b** are estimated to be 32.8 and 37.8 Å, respectively, whereas the Ru...Ru through-space distances between the two Ru centers in **5c** and **5d** are in the region 22-26 Å.

Electronic structure calculations on these model geometries reveal the HOMOs to be located mainly at the ethynylruthenium unit, whereas the LUMOs are on the porphyrin unit (Figures 6 and S12-S14). While the LUMOs are

essentially located on the porphyrin only in all cases, the porphyrin unit increasingly contributes to the HOMO on proceeding from **5a'** to **5d'**, with porphyrin characters of 5% (**5a'**),²⁴ 8% (**5b'**), 17% (**5c'**), and 21% (**5d'**). It is from the HOMO that the electron is lost following the initial oxidation, so the first oxidation is assigned to the ethynylruthenium unit, in line with CV data for all complexes **5a-5d**. In spite of the increase in number of the organometallic peripheral substituents when proceeding from **5a'** to **5d'**, the HOMO-LUMO gap increases only slightly (0.07 eV), while the HOMO is only slightly destabilized (0.10 eV).

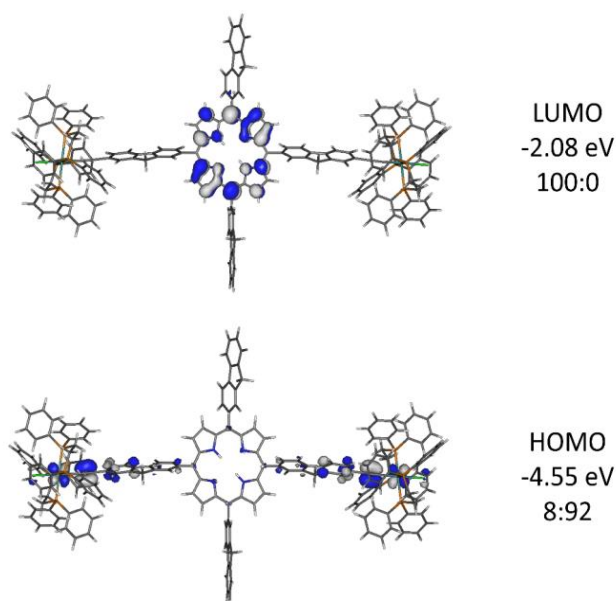


Figure 6. Frontier molecular orbitals for the optimised geometry of model **5b'** plotted with contour values of ± 0.03 ($e \text{ bohr}^{-3}$)^{1/2}. The ratios correspond to % orbital contributions on the porphyrin/fluorenyl groups and the $[-(\text{C}_{13}\text{H}_8\text{C}\equiv\text{C})\text{Ru}-\text{Cl}(\text{dppe})_2]$ fragments.

Photophysical properties

Linear optical properties. UV-Visible spectra were then measured for the two groups of compounds: the organic precursors (**7a-7d**) and the corresponding organometallic ruthenium adducts (**5a-5d**). As expected for free-base porphyrin derivatives, these two groups of compounds both exhibit very similar spectra, with intense Soret bands and four Q-bands in the UV-Vis range (Table 2 and Figure 7). Remarkably, no significant shifts of these characteristic absorptions are seen within each group, compared to the reference organic compound **6**, indicating a weak electronic influence of the peripheral organometallic end-groups on the porphyrin core. However, a clear feature of the spectra of **5a-5d** is the appearance of a new band between 350 and 400 nm which increases in intensity with the number of Ru(II) centers in the molecule. By analogy with previous work on related derivatives such as **12** or **13**,^{11, 17} but also on **5a**,²⁴ the latter can be attributed to a metal-to-ligand charge-transfer (MLCT) band (Figure 7b). The band at 350-400 nm in **5a** changes on oxidation of **5a** (analyzed by spectroelectrochemistry

elsewhere²⁴) and confirms the MLCT band assignments here for **5a-5d**. The modest shifts between these MLCT bands suggest that a weak electronic/excitonic coupling takes place between the branch-specific excitations.³⁹ Thus, the presence of an increasing number of metal centers is manifested in the 1PA spectra by the increase of this MLCT signature when progressing from **1a** to **1d**, in spite of the changes in symmetry experienced by certain conformers along this series.

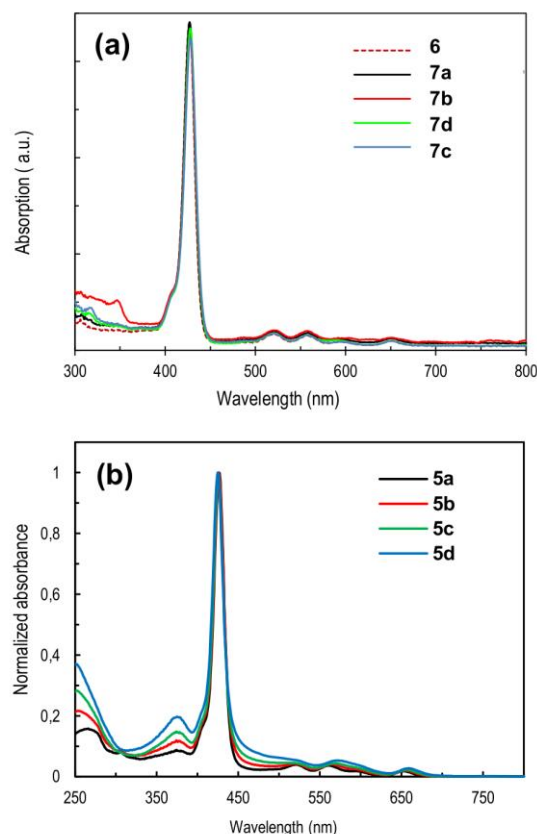


Figure 7. UV-Visible spectra of organic porphyrins **6**, **7a-7d** (a) and the corresponding ruthenium complexes **5a-5d** normalized on the Soret band (b) in CH_2Cl_2 at 20 °C.

As anticipated based on previous work,^{11, 23} in the presence of the Ru(II) endgroups,¹¹ the emission of the porphyrin core at ca. 660 nm and 725 nm is strongly quenched for **5a-5d** in CH_2Cl_2 solutions (ESI) compared to that previously found for the reference compound **6** (18%).³⁴ Thus, fluorescence quantum yields (Φ_F) below 1% are found for all organometallic derivatives, with Φ_F values decreasing from **5a** to **5d**, *i.e.* when increasing the number of Ru(II) substituents (ESI: Figure S15).³ Most likely, a “dark” MLCT state, located in energy slightly below the Q states,⁴ is at the origin of the luminescence trapping process in these Ru(II) derivatives.²⁴ In line with our

³ Accurate measurement of very low fluorescence quantum yields is problematic, since traces of non-metallated free-base precursor or related free bases might interfere.

⁴ Note, however, that the (vertical) transition to this dark state can occur at a slightly higher energy than the Q-band because of its significantly larger reorganisation energy.²⁴

DFT calculations, which indicate nearly constant HOMO and LUMO energy differences for **5a'**-**5d'**, and with the available redox data confirming the quite constant reduction and oxidation potentials observed for **5a-5d** (Table 1), this first MLCT state corresponding to a HOMO-LUMO excitation should be approximately isoenergetic for **5a-5d**.⁵

Table 2. Experimental UV-vis absorption maxima in CH₂Cl₂.

| Cmpd | λ_{\max} (nm) | | | | Ref. |
|-----------|------------------------|-------------|------------------|--------------------|--------------|
| | $\pi^* \leftarrow \pi$ | MLCT | Soret | Q bands | |
| 1b | nd ^a | 330 | 421 ^b | 563, 612 | 17 |
| 5a | 262,310 | 365 | 427 | 520, 559, 593, 649 | 24 |
| 5b | 275 | 374 | 426 | 520, 565, 588, 653 | ^c |
| 5c | 275 | 374 | 425 | 515, 573, 657 | ^c |
| 5d | 282 | 375 | 426 | 522, 567, 658 | ^c |
| 6 | 280 | / | 426 | 519, 555, 592, 652 | 34 |
| 7a | 283 | / | 428 | 519, 556, 596, 652 | 32 |
| 7b | 288 | / | 427 | 520, 558, 604, 650 | ^c |
| 7c | 290 | / | 428 | 520, 556, 592, 653 | ^c |
| 7d | 292 | / | 428 | 520, 558, 594, 652 | 34 |
| 12 | nd | 327, 452 | 418 | 563, 615 | 17 |
| 13 | / | 373 | / | / | 36 |

^a Not determined. ^b Weak shoulder at 460 nm. ^c This work.

Nonlinear optical properties. Nonlinear absorption and nonlinear refraction properties for **5a-5d** were determined in the 650-1200 nm range by femtosecond Z-scan studies (Figure 8 and ESI).

Real and imaginary parts of the third-order nonlinear response. The real part (γ_{re}) of the third-order molecular nonlinear refraction coefficient (γ) at a given wavelength is obtained from the closed-aperture Z-scan measurement, while its imaginary part (γ_{im}) is obtained from the open-aperture measurement. Consistent with our previous measurements on related organometallics, nonlinear refraction (γ_{re}) dominates the cubic NLO response over the spectral range probed (ESI: Figure S16).^{11, 20} The γ_{re} values are negative and consistently

⁵ Based on the weak excitonic coupling previously seen between the MLCT transitions at higher energy, near 290 nm (and supported by the weak intermetallic coupling in the mixed-valent states indicated by the CV studies), we believe that the energies of these new MLCT bands should only be modestly affected by changes in symmetry along the series **5a-5d** (as should also be the case for the 2PA properties).

larger in magnitude than the nonlinear absorption coefficients (γ_{im}). For all four compounds in the spectral range 650-1200 nm, the maximal $|\gamma_{re}|$ values lie between 650 and 680 nm, a region in which γ_{re} is certainly resonance enhanced. Values for **5a-5d** are similar (ca. -2000-3000 x 10⁻³⁴ esu with $|\gamma_{im}|$ values below 500 x 10⁻³⁴ esu), meaning that a roughly two-fold decrease in the weighted $|\gamma|/M$ datum is found proceeding from **5a** to **5b** (from 1.228 to 0.558 x 10⁻³⁴ esu.mol/g). These values are lower than those previously found for porphyrin **3**²⁰ but significantly higher than those of **1b** or **13**³⁶ (ESI: Table S1). Given the importance of nonlinear absorption for various applications involving tetrapyrrolic macrocycles,^{12, 14, 40} its evolution was examined more closely for **5a-5d**.

Nonlinear absorption. Organometallic porphyrins **5a-5d** display pronounced nonlinear absorption in several spectral ranges (Figure 8). Effective 2PA cross-sections (σ_2) have been derived for all of them (Table 3). Large effective cross-sections (σ_2) were found at wavelengths less than 700 nm with very large error margins. There is significant linear absorption in this specific spectral range, resulting in excited-state absorption (ESA) as well as two-photon absorption (2PA) and so the 2PA in this spectral range is convoluted with ESA (saturable absorption (SA) or reverse saturable absorption (RSA)), complicating the interpretation of these data.⁴³ We have therefore not focused on data corresponding to wavelengths below 800 nm and have restricted our analysis to the longer wavelength range where there is no/minimal linear absorption. The compounds also display several nonlinear absorption maxima at longer wavelengths, beyond the 1PA region, in particular at 850-875 nm and 930-950 nm. In spite of the likely presence in solution of centrosymmetric rotamers for **5b** and **5d**, in principle subject to the exclusion rule,¹ a fair match between the 1PA (plotted at twice the wavelength) and the 2PA spectra can be observed for all compounds **5a-5d**.

Comparison with the 1PA spectra reveals that these maxima correspond well with twice the wavelength of the Soret band, and twice that of the first Q-band (Figure 8). These bands seem therefore to correspond to excitation to the states that are populated by the 2PA processes.⁷ Although the maxima at ca. 925-950 nm are at a wavelength that roughly correspond to 2PA into one of the Q bands, the 2PA at these wavelengths more likely corresponds to excitation into the first MLCT state, which is hidden beneath the Q bands. As mentioned above, this MLCT state is believed to be at the origin of the luminescence trapping process in **5a-5d**. For the Ru(II) derivative **5a**, the MLCT process is assumed to give rise to a weak band located at ca. 510 nm,²⁴ and this state should be essentially isoenergetic with those in **5b-5d**. Because of the different selection rules operative in 2PA and 1PA, this state could be at the origin of the intense 2PA maxima observed for **5a-5d** at ca. 930-950 nm. If this assignment is correct, the 2PA peaks detected confirm that the "hidden" MLCT bands are located at slightly higher energies (shorter wavelengths) than the first Q band.

Table 3. Experimental γ_{re} , γ_{im} , $|\gamma|$, and σ_2 values in CH_2Cl_2 at selected wavelengths^a corresponding to extrema of the nonlinear absorption spectra of **5a-5d**, and comparison to data previously obtained for **1b**²⁰ and **13**.³⁶

| Cmpd | λ^b | γ_{re}^c | γ_{im}^c | $ \gamma ^c$ | σ_2^d | $[\sigma_2/(N_{eff})^2]^e$ | $[\sigma_2/M]^f$ |
|-----------|-------------|---------------------------------|-----------------|-----------------|------------------|----------------------------|------------------|
| 1b | 900 | Data not measured ¹⁷ | | | 1100 ± 50 | 0.28 ± 0.01 | 0.23 ± 0.01 |
| 5a | 850 | -1400 ± 350 | 350 ± 130 | 1500 ± 350 | 7500 ± 2800 | 1.5 ± 0.6 | 3.2 ± 1.2 |
| | 935 | -1150 ± 150 | 610 ± 150 | 1300 ± 200 | 11000 ± 2900 | 2.2 ± 0.6 | 4.7 ± 1.2 |
| | 1125 | -550 ± 80 | 150 ± 30 | 600 ± 90 | 1900 ± 400 | 0.4 ± 0.1 | 0.8 ± 0.2 |
| 5b | 850 | -1000 ± 350 | 450 ± 200 | 1100 ± 400 | 10000 ± 4500 | 1.8 ± 0.8 | 3.0 ± 1.4 |
| | 930 | -1150 ± 150 | 610 ± 160 | 1300 ± 200 | 11000 ± 3000 | 2.0 ± 0.5 | 3.3 ± 0.9 |
| | 1150 | -1700 ± 1500 | 290 ± 300 | 1700 ± 1600 | 3400 ± 3500 | 0.6 ± 0.6 | 1.0 ± 1.0 |
| 5c | 875 | -1600 ± 200 | 570 ± 140 | 1650 ± 250 | 14000 ± 3500 | 2.3 ± 0.6 | 3.3 ± 0.8 |
| | 950 | -2100 ± 550 | 950 ± 350 | 2300 ± 650 | 16200 ± 5700 | 2.7 ± 0.9 | 3.8 ± 1.3 |
| | 1150 | -530 ± 90 | 170 ± 40 | 550 ± 100 | 2000 ± 450 | 0.3 ± 0.1 | 0.5 ± 0.1 |
| 5d | 875 | -1400 ± 200 | 800 ± 200 | 1600 ± 250 | 16000 ± 4000 | 2.4 ± 0.6 | 3.0 ± 0.8 |
| | 950 | -1600 ± 450 | 1120 ± 500 | 2000 ± 700 | 21000 ± 9000 | 3.1 ± 1.3 | 3.9 ± 1.7 |
| | 1150 | -500 ± 150 | 450 ± 150 | 650 ± 200 | 5500 ± 1800 | 0.8 ± 0.3 | 1.0 ± 0.3 |

^a Conditions: measurements were carried out in CH_2Cl_2 ; γ values are referenced to the nonlinear refractive index of silica $n_2 = 2.92 \times 10^{-16} \text{ cm}^2 \text{ W}^{-1}$. ^b Wavelength of the laser in nm. ^c 10^{-34} esu. The SI units for γ are $\text{C m}^4 \text{ V}^{-3}$, while those in the cgs system (used almost exclusively in the literature, and so given here) are $\text{cm}^5 \text{ statV}^{-2}$ or esu. To convert between the two systems, $\gamma_{\text{SI}} = (1/3)^4 \times 10^{-23} \gamma_{\text{cgs}}$. ^d Effective (apparent) 2PA cross-section in Göppert-Mayer units ($1 \text{ GM} = 1 \times 10^{-50} \text{ cm}^4 \text{ s photon}^{-1}$). ^e σ_2 corrected for the squared effective number of electrons (N_{eff}^2).^{41, 42} ^f $|\sigma_2|$ corrected for the molecular mass (M in g mol^{-1}). ^g No error estimated.

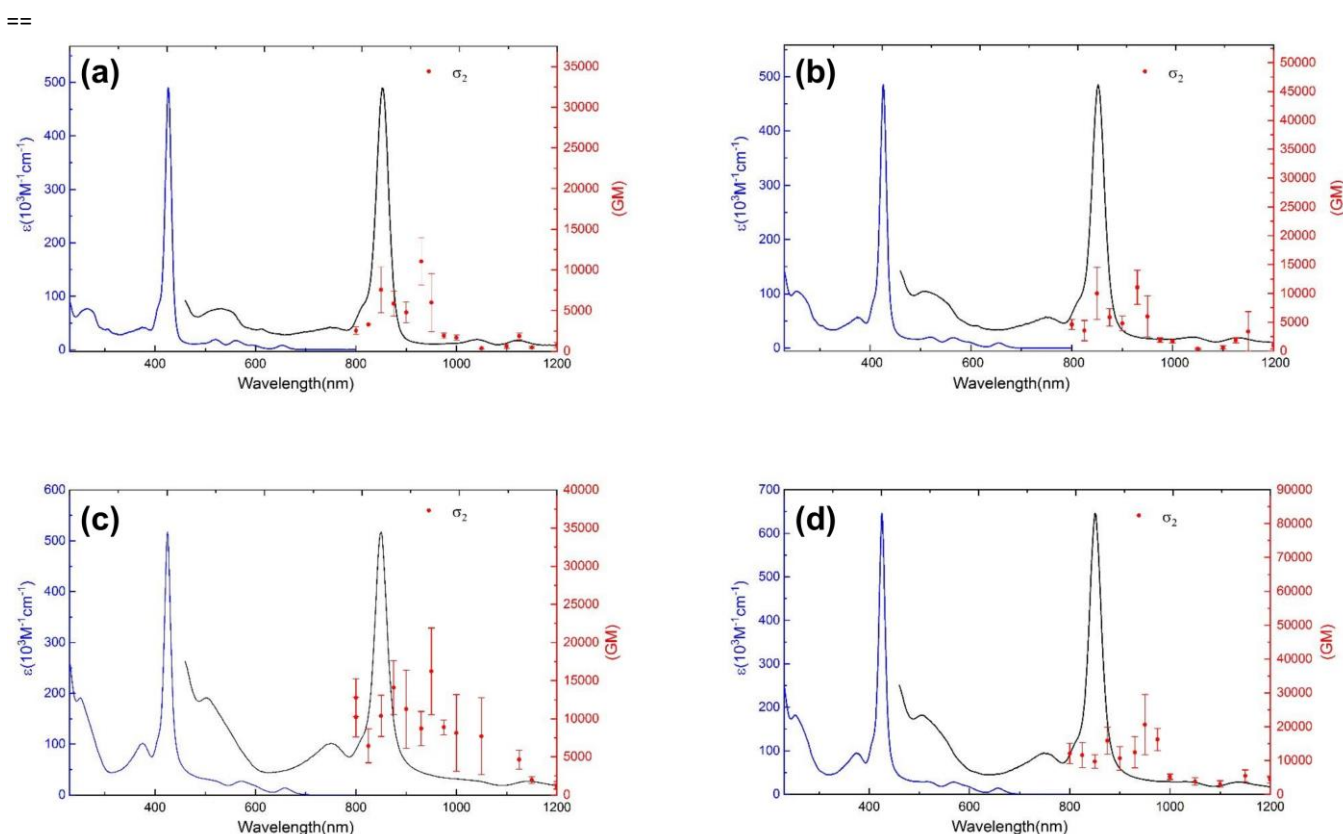


Figure 8. Two-photon absorption cross-section plots (red) for **5a** (a), **5b** (b), **5c** (c) and **5d** (d) overlaid on the one-photon absorption (1PA) spectra (blue) and the same 1PA spectra plotted at twice the wavelength (black).

We are unsure of the nature of the remaining (and weaker) 2PA maxima detected around 1125-50 nm. We notice that they would nicely correspond to two times the wavelengths of some of the Q bands. Given that there are precedents for three-photon absorption into MLCT states with Ru(II) alkynyl complexes,⁷ we examined the data closely, but they are consistent with 2PA and not 3PA.⁶

At wavelengths above 800 nm, the maxima, which are believed to originate from pure 2PA, display comparatively large σ_2 values,¹ especially when compared to those of organic free-base porphyrins of similar size^{42, 44} (for which 2PA corresponding to MLCT states cannot occur). As previously discussed,¹⁷ simple Zn(II) porphyrins usually show very weak 2PA (< 50 GM) at wavelengths greater than 700 nm which is believed to originate from a porphyrin-based dark excited state with an energy just above that of the Soret band.⁴⁵ As a result, purely organic porphyrin-based arrays exhibiting 2PA above 1000 nm remain rare.⁴⁴ Thus, no such third-order NLO activity was previously detected for ZnTPP at 1024 nm by Boudebs *et al.* using dark field Z-scan (DFZ-scan),⁴³ revealing the beneficial influence of metalation by [*trans*-RuCl(dppe)₂(C≡C)]- endgroups for promoting nonlinear absorption in the near-IR range. Furthermore, we clearly show here with **5a-5d** that increasing the level of "ruthenation" at the periphery correlates with an increase in the effective cross-sections of the various maxima detected. For these four compounds, if the cross-sections of the 2PA transitions at 925-950 nm (presumed to involve the MLCT states) are scaled by the number of Ru(II) end-groups, the values are still larger than that for 2PA into the MLCT state of the corresponding model complex **13** (360 GM). This clearly indicates that nonlinear absorption cannot be solely attributed to the metallated peripheral arms, but that synergy with the porphyrin core exists.

To understand better the origin of these nonlinear absorptions, we have corrected their cross-sections by the square of the effective number of electrons (N_{eff}^2). Such a figure of merit explicitly takes into consideration the contribution of the electrons present in various π -manifolds on NLO properties, although the lone pairs or the d electrons on the metal centres are not considered in the approach originally proposed by Kuzyk *et al.*⁴¹ We have derived the N_{eff} values using this approach, considering the peripheral ligands to be fully conjugated with the central porphyrin ring (ESI Table S2). The corresponding figures of merit for the compounds were then computed from the 2PA cross-sections (Table 3).⁷ For a given 2PA maximum, these figures appear to increase slightly

when progressing from **5a** to **5d**. Thus, the increase seen for the σ_2 values between **5a** to **5d** is not just due to the additional π -electrons introduced via the co-ligands and alkynyl ligands at the organometallic end-group(s). Other parameters resulting from the extension of the π -manifold (*e.g.* reduction of the energy gaps between relevant MOs involved in the 2PA transition) or from the presence of metal centers (*e.g.* additional polarizable d⁸ electrons, not presently accounted for in the N_{eff} values) seem to be operative.^{8,16} This statement certainly justifies *a posteriori* the need to take better account of the active d_{Ru} electrons when determining the N_{eff} value for organometallic molecules incorporating such Ru(II) alkynyl complexes as endgroups or connectors.⁴⁶ Finally, correcting σ_2 values for the molecular mass of the molecules provides a quick indirect means to evaluate the dependence of 2PA on the molecular size. Again, a global increase in this figure of merit is seen for a given 2PA transition between **5a** and **5d**, which is not surprising given that good linear correlations are seen between this figure of merit and the previous one for the compounds under consideration (ESI, Figure S17). Besides confirming that the saturation limit has not yet been reached upon peripheral metallation of the H₂TFP core in **5d**, these figures of merit will also allow selection of the most efficient (by mass or volume) nonlinear absorbers among **5a-5d** in a wavelength range above 700 nm, important information for potential applications such as optical power limiting.⁴⁷

3. Conclusions

We have reported herein the synthesis of four new members of a series of *meso*-tetra(fluorenyl)porphyrin derivatives featuring one to four *trans*-RuCl(κ^2 -dppe)₂ alkynyl complexes σ -linked at their periphery (**5a-5d**). While the third-order nonlinear responses of all these compounds are strongest around 700 nm (with negative cubic polarizability coefficients χ), they also exhibit sizeable nonlinear absorption properties extending into the near-IR range. In this study, besides confirming the systematic existence of these nonlinear absorption peaks at low energy, we now also (i) demonstrate that their effective cross-sections are directly dependent on the number of metallic centres present at the periphery and, for the first time, (ii) propose a rationale for explaining their physical origin. Furthermore, when **5a-5d** are compared to known related organometallic porphyrins, the tetrametallic free-base derivative **5d** appears to be more NLO-active than its tetraphenyl Zn(II) analogue **1b**. This reveals the existence of a synergy between the organometallic termini and the central porphyrin core, since the latter promotes the 2PA activity. In this respect, the better performance of **5d** compared to **1b** can

⁶ These bands were checked for possible 3PA, but despite roughly correlating with three-times the wavelength of the MLCT band near 380 nm, the shapes of the Z-scan traces are inconsistent with 3PA.

⁷ Qualitatively similar statements can be made using N_{eff} values (ESI, Table S2) derived for porphyrin compounds in which the π -manifold on the peripheral arms are considered as non-interacting (disconnected) and including (or not) all π -electron of the ligands on the peripheral Ru(II) complexes.

⁸ N_{eff} values were derived for the various porphyrins by considering that the four *meso*-branches were fully interacting with the porphyrin core (see ESI). Thus, they correspond to an upper limit for evaluating the impact of the π -electrons in these compounds, since the π -systems of the *meso*-branches are canted with respect to the central core for steric reasons (*i.e.* they adopt non co-planar conformations).

be related to the extension of the central π -manifold. In addition, with the help of relevant figures of merit, we also show that *all* d⁶-transition metal complexes contribute to enhancement of the near-IR 2PA (MPA) properties in **5a-5d**.

As a result, and in line with previous contributions of our groups, this study confirms that peripheral metallation by electron-rich Ru(II) alkynyl complexes at a (central) tetra(aryl)porphyrin ring constitutes a general and efficient method to enhance 2PA in the near-IR range.⁹ Given the strategic importance of the 1000-1500 nm spectral range (also known as the “telecommunications window”) for various applications, we hope that such approaches will prove helpful in the design of new nonlinear absorbers based on tetrapyrrolic macrocycles.

4. Experimental

Synthetic procedures

General. Unless otherwise stated, all solvents used in reactions were distilled using common purification protocols,⁴⁸ except for DMF and iPr₂NH which were dried over molecular sieves (3 Å). Compounds were purified by chromatography on silica gel using different mixtures of eluents as specified. ¹H and ¹³C NMR spectra were recorded on Bruker Ascend 400 and 500 MHz spectrometers at 298 K (for labelling of nuclei, see Figure 3). The chemical shifts are given in ppm and referenced to internal tetramethylsilane. Cyclic voltammograms were recorded with an Autolab PG-STAT 30 potentiostat at 20 °C from solutions of *ca.* 10⁻⁴ M analyte in dry dichloromethane containing 0.1 M [Bu₄N][PF₆] at a scan rate $\nu = 100 \text{ m s}^{-1}$ under a dry nitrogen atmosphere. The single compartment three-electrode cell was equipped with platinum wire counter and reference electrodes and a glassy carbon working electrode. Redox potentials were measured using the decamethylferrocene/decamethylferrocenium (Cp*₂Fe⁺/Cp*₂Fe) redox couple as an internal reference system at -0.53 V⁴⁹ vs. the usual ferrocene/ferrocenium (Cp₂Fe⁺/Cp₂Fe) redox couple in CH₂Cl₂ set at 0.46 V.³⁷ Solutions were purged and maintained under a nitrogen atmosphere. High-resolution mass spectra (HRMS) were recorded on different spectrometers: a Bruker MicroTOF-Q II, a Thermo Fisher Scientific Q-Exactive in ESI positive mode and a Bruker Ultraflex III MALDI Spectrometer at CRMPO (centre regional de mesures physiques de l'Ouest) in Rennes. Reagents were purchased from commercial suppliers and used as received. The [RuCl(dppe)₂][PF₆] salt (**8**[PF₆]),^{35, 50} 9,9-dibutyl-9H-fluorene-2-carbaldehyde (**10**)³⁰

and 7-((trimethylsilyl)ethynyl)-9,9-dibutyl-9H-fluorene-2-carbaldehyde (**11**)³² were prepared as described earlier.

Synthesis of organic porphyrins 6 and 7a-7d. In a two-necked flask, a mixture of 9,9-dibutyl-fluorene-2-carbaldehyde (2.1 g, 6.7 mmol, 3 equiv), 9,9-dibutyl-7-((trimethylsilyl)ethynyl)-fluorene-2-carbaldehyde (900 mg, 2.2 mmol, 1 equiv) and pyrrole (0.6 mL, 8.9 mmol, 4 equiv.) was dissolved in dry chloroform (550 mL) under argon. After deoxygenating the mixture via argon bubbling for 30 min, BF₃•OEt₂ (0.2 mL) was injected and the reaction was stirred in the dark for 3 h under argon at room temperature. *p*-Chloranil (1.5 g, 6.1 mmol) was then added as oxidant and the reaction was heated at 60 °C for another 2 h in air. After cooling the reaction to room temperature, NEt₃ (2 mL) was injected, and the medium was kept stirring for 10 min. After evaporation of the volatiles, purification was carried out by silica chromatography using a CH₂Cl₂/heptane (1:3) mixture as eluent. The various porphyrin isomers **9a-9d** could not be separated and were thus collected together and isolated as a red solid. This mixture (3.6 g, 2.5 mmol) was then dissolved in a CH₂Cl₂/THF/MeOH (3:1:1) solvent mixture and K₂CO₃ (2.0 g, 14.5 mmol) was added with stirring at 60 °C for 10 h. After stirring overnight, the volatiles were removed *in vacuo* and the resulting mixture of desilylated porphyrins **7a-7d** was purified by chromatography on silica gel, using heptane/THF (4:1) and then heptane/THF (10:1) mixtures as eluents.

Porphyrin 6. Yield: 44%.²⁸ ¹H NMR (400 MHz, CDCl₃): $\delta = 8.92$ (s, 8H, *H* _{β -pyr), 8.26-8.18 (m, 8H, *H*_{1,3}), 8.07 (d, 4H, *J* = 7.5 Hz, *H*₄), 7.96 (d, 4H, *J* = 7.3 Hz, *H*₄), 7.52-7.41 (m, 12H, *H*_{6,7,8}), 2.14 (t, *J* = 7.2 Hz, 16H, *H*_a), 1.21-1.14 (m, 16H, *H*_c), 1.02-0.87 (m, 16H, *H*_b), 0.78-0.72 (m, 24H, *H*_d), -2.57 (s, 2H, NH).}

Porphyrin 7a. Yield: 17%.³²

Porphyrin 7b. Yield: 8%. ¹H NMR (400 MHz, CDCl₃): $\delta = 8.91$ (d, 8H, *J* = 9.1 Hz, *H* _{β -pyr), 8.23-8.18 (m, 8H, *H*_{1,3}, *H*_{1'}, *H*_{3'}), 8.08-8.06 (m, 4H, *H*₄, *H*_{4'}), 7.96 (d, 2H, *J* = 7.2 Hz, *H*₅), 7.91 (d, 2H, *J* = 7.7 Hz, *H*_{5'}), 7.63 (d, 4H, *J* = 8.0 Hz, *H*₆, *H*₈), 7.52-7.41 (m, 6H, *H*_{6,7,8}), 3.21 (s, 2H, *H*₇), 2.14 (s, 16H, *H*_a), 1.21-1.14 (m, 16H, *H*_c), 0.99-0.85 (m, 16H, *H*_b), 0.78-0.73 (m, 24H, *H*_d), -2.58 (s, 2H, NH). ¹³C{¹H} NMR (100 MHz, CDCl₃): $\delta = 151.2, 149.6, 149.2, 141.8, 141.6, 140.9, 140.8, 140.7, 139.9, 133.8, 133.6, 131.5, 129.4, 129.3, 127.4, 127.0, 126.7, 123.1, 120.9, 120.9, 120.6, 120.5, 120.5, 120.1, 120.0, 118.3, 117.8, 84.7, 55.4, 55.5, 40.3, 40.2, 26.3, 23.1, 14.0, 13.9$. HRMS-MALDI (DCTB): *m/z* = 1462.895 [M]⁺ (calcd for [C₁₀₈H₁₁₀N₄]⁺: 1462.8725). **Anal.** Calcd. (%) for C₁₀₈H₁₁₀N₄•EtOH: C, 87.49; H, 7.74; N, 3.71. Found: C, 87.58; H, 7.76; N, 3.48.}

Porphyrin 7c. Yield: 2%. ¹H NMR (400 MHz, CDCl₃): $\delta = 8.93$ -8.90 (m, 8H, *H* _{β -pyr), 8.25-8.18 (m, 8H, *H*_{1,3}, *H*_{1'}, *H*_{3'}), 8.07 (d, 4H, *J* = 7.2 Hz, *H*₄, *H*_{4'}), 7.96 (d, 1H, *J* = 7.2 Hz, *H*₅), 7.91 (d, 3H, *J* = 7.6 Hz, *H*_{5'}), 7.63 (d, 3H, *J* = 8.0 Hz, *H*₆, *H*₈), 7.51-7.41 (m, 3H, *H*_{6,7,8}), 3.21 (s, 3H, *H*₇), 2.13 (s, 16H, *H*_a), 1.22-1.14 (m, 16H, *H*_c), 0.91-0.84 (m, 16H, *H*_b), 0.79-0.73 (m, 24H, *H*_d), -2.59 (s, 2H,}

⁹ Note that the impact of these organometallic endgroups on the NLO properties is not always directly related to their electron-releasing capability in the ground state,⁸ but rather to their involvement in the low-energy excited states (MLCT states here), which determine the nonlinear polarization and absorption properties of a given molecule.

NH). $^{13}\text{C}\{^1\text{H}\}$ NMR (100 MHz, CDCl_3): δ = 151.2, 149.6, 149.2, 141.8, 141.6, 140.9, 140.8, 140.8, 139.9, 133.8, 133.6, 131.5, 129.4, 129.3, 127.4, 127.0, 126.7, 123.1, 121.0, 120.9, 120.6, 120.6, 120.5, 120.1, 120.0, 118.3, 117.8, 84.7, 55.4, 55.3, 40.3, 40.2, 26.3, 23.1, 14.0, 13.9. **Anal. Calcd.** (%) for $\text{C}_{110}\text{H}_{110}\text{N}_4 \cdot \text{EtOH}$: C, 87.68; H, 7.62; N, 3.65. Found: C, 87.58; H, 7.76; N, 3.48.

Porphyrin 7d. Yield: 1%.³⁴

Synthesis of organoruthenium porphyrins 5a-5d. In a Schlenk tube, a mixture of the desired porphyrin precursor (**5b-5d**) (40 mg, 0.03 mmol, 1 equiv.), *n* equiv. (*n* corresponding to the number of terminal alkynes in **5b-d**) of the $[\text{RuCl}(\text{dppe})_2][\text{PF}_6]$ salt (*n* x 32 mg, *n* x 0.03 mmol) and NaPF_6 (*n* x 5 mg, *n* x 0.1 mmol, *n* equiv.) were stirred in distilled CH_2Cl_2 under argon at 20 °C. The reaction medium was deoxygenated by argon bubbling for 10 min and the reaction was kept stirring for 96 h at room temperature, after which NEt_3 was injected to complete the reaction and stirring maintained 2 h more under argon. After evaporation of the volatiles, the residue was purified by chromatography on basic Al_2O_3 using $\text{CH}_2\text{Cl}_2/\text{NEt}_3$ (100:1) as eluent, providing fractions of the various title porphyrin derivatives in a pure state.

Porphyrin 5a. Yield: 63%.²⁴

Porphyrin 5b. Yield: 60%. ^1H NMR (400 MHz, CDCl_3): δ = 8.97-8.93 (m, 8H, $H_{\beta\text{-pyr}}$), 8.27-8.16 (m, 8H, H_{flu}), 8.10-8.09 (m, 2H, H_{flu}), 7.99-7.97 (m, 4H, H_{flu}), 7.72-7.71 (m, 3H, $H_{\text{Ph-dppe}}$), 7.59-7.58 (m, 14H H_{flu} , $H_{\text{Ph-dppe}}$), 7.52-7.42 (m, 9H, H_{flu} , $H_{\text{Ph-dppe}}$), 7.35-7.33 (m, 15H, H_{flu} , $H_{\text{Ph-dppe}}$), 7.24-7.19 (m, 15H, $H_{\text{Ph-dppe}}$), 7.04-6.98 (m, 28H, $H_{\text{Ph-dppe}}$), 6.79 (d, 4H, J = 7.8 Hz, $H_{\text{Ph-dppe}}$), 5.59 (s, 4H, $H_{\text{Ph-dppe}}$), 2.76 (s, 12H, $\text{CH}_2\text{-dppe}$), 2.58-2.52 (m, 4H, $\text{CH}_2\text{-dppe}$), 2.23-2.03 (m, 16H, H_a), 1.06-0.96 (m, 16H, H_a), 0.90-0.71 (m, 40H, H_b , H_d), -2.49~-2.61 (m, 2H, NH). $^{31}\text{P}\{^1\text{H}\}$ NMR (100 MHz, CDCl_3): δ = 49.4 (s, 8P, $P_{(\text{dppe})_2}$). **HRMS-ESI** ($\text{CHCl}_3/\text{HCO}_2\text{H}$): m/z = 1663.5735 $[\text{M}]^{2+}$ (calcd for $[\text{C}_{212}\text{H}_{204}\text{N}_4\text{P}_8\text{Ru}_2\text{Cl}_2]^{2+}$: 1663.5720), 3327.1438 $[\text{M}]^{+}$ (calcd for $[\text{C}_{212}\text{H}_{204}\text{N}_4\text{P}_8\text{Ru}_2\text{Cl}_2]^{+}$: 3327.1446).

Porphyrin 5c. Yield: 60%. ^1H NMR (400 MHz, CDCl_3): δ = 8.99-8.93 (m, 8H, $H_{\beta\text{-pyr}}$), 8.29-8.16 (m, 8H, H_{flu}), 8.11-8.07 (m, 1H, H_{flu}), 8.01-7.96 (m, 4H, H_{flu}), 7.82-7.78 (m, 1H, H_{flu}), 7.72 (d, 3H, J = 7.5 Hz, $H_{\text{Ph-dppe}}$), 7.67-7.55 (m, 21H H_{flu} , $H_{\text{Ph-dppe}}$), 7.52-7.38 (m, 10H, H_{flu} , $H_{\text{Ph-dppe}}$), 7.37-7.30 (m, 24H, H_{flu} , $H_{\text{Ph-dppe}}$), 7.25-7.20 (m, 21H, $H_{\text{Ph-dppe}}$), 7.05-6.99 (m, 46H, $H_{\text{Ph-dppe}}$), 6.80 (d, 5H, J = 8.3 Hz, $H_{\text{Ph-dppe}}$), 5.85 (t, 1H, J = 8.3 Hz, $H_{\text{Ph-dppe}}$), 3.55-3.51 (m, 2H, $\text{CH}_2\text{-dppe}$), 2.76 (s, 22H, $\text{CH}_2\text{-dppe}$), 2.29-2.06 (m, 16H, H_a), 1.08-1.05 (m, 16H, H_c), 0.91-0.72 (m, 40H, H_b , H_d), -2.49~-2.57 (m, 2H, NH). $^{31}\text{P}\{^1\text{H}\}$ NMR (100 MHz, CDCl_3): δ = 49.5 (s, 12P, $P_{(\text{dppe})_2}$). **HRMS-ESI** ($\text{CHCl}_3/\text{HCO}_2\text{H}$): m/z = 1428.4280 $[\text{M}]^{3+}$ (calcd for $[\text{C}_{266}\text{H}_{251}\text{N}_4\text{P}_{12}\text{Ru}_3\text{Cl}_3]^{3+}$: 1428.4296), 2142.6377 $[\text{M}]^{2+}$ (calcd for $[\text{C}_{266}\text{H}_{251}\text{N}_4\text{P}_{12}\text{Ru}_3\text{Cl}_3]^{2+}$: 2142.6447).

Porphyrin 5d. Yield: 61%. ^1H NMR (400 MHz, CDCl_3): δ = 8.99 (s, 8H, $H_{\beta\text{-pyr}}$), 8.26-8.18 (m, 8H, H_{flu}), 8.02-7.99 (m, 4H, H_{flu}),

7.72 (d, 4H, J = 7.6 Hz, H_{flu}), 7.61-7.59 (m, 31H, H_{flu} , $H_{\text{Ph-dppe}}$), 7.35-7.33 (m, 31H, H_{flu} , $H_{\text{Ph-dppe}}$), 7.24-7.19 (m, 32H, $H_{\text{Ph-dppe}}$), 7.04-7.00 (m, 70H, $H_{\text{Ph-dppe}}$), 6.80 (d, 8H, J = 8.5 Hz, $H_{\text{Ph-dppe}}$), 2.76 (s, 32H, $\text{CH}_2\text{-dppe}$), 2.20-2.09 (m, 16H, H_a), 1.08-0.99 (m, 16H, H_c), 0.89-0.83 (m, 40H, H_b , H_d), -2.47 (m, 2H, NH). $^{31}\text{P}\{^1\text{H}\}$ NMR (100 MHz, CDCl_3): δ = 49.5 (s, 16P, $P_{(\text{dppe})_2}$). **HRMS-ESI** ($\text{CHCl}_3/\text{HCO}_2\text{H}$): m/z = 1310.6095 $[\text{M}]^{4+}$ (calcd for $[\text{C}_{320}\text{H}_{298}\text{N}_4\text{P}_{16}\text{Ru}_4\text{Cl}_4]^{4+}$: 1310.6066), 1747.4765 $[\text{M}]^{3+}$ (calcd for $[\text{C}_{320}\text{H}_{298}\text{N}_4\text{P}_{16}\text{Ru}_4\text{Cl}_4]^{3+}$: 1747.4757), 2621.2119 $[\text{M}]^{2+}$.

Computations. All computations were carried out with the Gaussian 09 package.⁵¹ The S_0 model geometries of **5b'**, **5c'** and **5d'** with no symmetry constraints were optimized with the B3LYP functional⁵² using the 3-21G* basis set⁵³ for all atoms. The MO diagrams in Figures 6 and S10-12 were generated with the Gabedit package⁵⁴ and the %MO contributions were determined using the GaussSum software.⁵⁵

Absorption and emission studies. All photophysical measurements were performed with freshly-prepared air-equilibrated solutions at room temperature (298 K). UV-Vis absorption spectra were recorded on a BIO-TEK instrument UVIKON XL spectrometer or on a Jasco V-570 spectrophotometer. PL emission was recorded on a Photon Technology International (PTI) apparatus coupled to an 814 Photomultiplier Detection System, Lamp Power Supply 220B and MD-5020. Steady-state fluorescence measurements were performed on dilute solutions (*ca.* 10^{-6} M, optical density < 0.1) contained in standard 1 cm quartz cuvettes using an Edinburgh Instruments (FLS920) spectrometer in photon-counting mode, equipped with a calibrated quantum counter for excitation correction. Fully corrected emission spectra were obtained, for each compound, after excitation at the wavelength of the absorption maximum, with $A_{\lambda_{\text{ex}}} < 0.1$ to minimise internal absorption. Fluorescence quantum yields were measured using standard methods; TPP in CH_2Cl_2 ($\Phi_{\text{lum}} = 0.12$ at $\lambda_{\text{ex}} = 417$ nm) was used as a reference.

Z-scan studies. Wavelength-dependent Z-scan experiments were obtained using a light source consisting of a Quantronix Integra-C3.5F laser pumping a Quantronix Palitra-FS optical parametric amplifier, tuneable over a wavelength range from 500 nm to 2000 nm. The output was confirmed by use of an Ocean Optics USB2000+ spectrometer (500-1000 nm) or an Ocean Optics NIR-Quest spectrometer (1000-1800 nm). The output delivered 130 fs pulses with a 1 kHz repetition rate. Colored glass filters and a Thorlabs polarizing filter were used to remove unwanted wavelengths. The power was adjusted by use of neutral density filters to obtain nonlinear phase shifts between 0.2 to 1.3 rad. The focal length of the beam at the experiment was 100 mm for wavelengths between 500 and 950 nm, and 75 mm from 1000-1800 nm, which gave 35-50 μm beam waists resulting in Rayleigh lengths longer than that of the sample thickness. Samples travelled down the Z axis on a Thorlabs motorized stage between 0-40 mm or 50-100 mm, depending on the focal length. Data were collected by two Thorlabs photodiodes, 500-900 nm with Si based detectors

and 900-1800 nm with InGaAs detectors. Data from the detectors were collected by a Tektronix oscilloscope feeding a custom LabVIEW program permitting fitting of a theoretical trace. A sample of CH₂Cl₂ was run at each wavelength as an aid in referencing to the response from a 3 mm fused silica plate (also run at each wavelength). Solutions of the chromophores were analyzed in deoxygenated and distilled CH₂Cl₂ at concentrations 0.09, 0.15, 0.14 and 0.13 wt% for **5a-5d**, respectively, placed in 1 mm glass cells. The real and imaginary components of the second hyperpolarizability (γ) of the materials were calculated assuming additivity to these reference samples, and γ_{im} was used to calculate the two-photon absorption cross sections (σ_2).

Conflicts of interest

There are no conflicts to declare.

Acknowledgements

This research was supported by grants from MEAE and MESRI (PHC FASIC Chercheurs 2019, Project N° 43406ZE), from the Australian Research Council (M.G.H., DP170100408), from Durham University, and from the CNRS (LEA Rennes-Durham, PICS program 7106 and LIA Redochrom). The China Scholarship Council (CSC) is also acknowledged for PhD funding (CSC) (X.Z. and L.S.). J. A. G. Williams (Durham) is kindly acknowledged for discussion and fluorescence measurements.

References

- G. S. He, L.-S. Tan, Q. Zheng and P. N. Prasad, *Chem. Rev.*, 2008, **108**, 1245-1330.
- G. S. He, J. D. Bhawalkar, C. F. Zhao, C. K. Park and P. N. Prasad, *Opt. Lett.*, 1995, **20**, 2393-2395.
- D. A. Parthenopoulos and P. M. Rentzepis, *Science*, 1989, **245**, 843-845.
- a) S. Kawata, H.-B. Sun, T. Tanaka and K. Takada, *Nature*, 2001, **412**, 697-698; b) C. R. Mendonca, D. S. Correa, F. Marlow, T. Voss, P. Tayalia and E. Mazur, *Appl. Phys. Lett.*, 2009, **95**, 113309 (1-3).
- a) T. J. Dougherty and S. L. Marcus, *Eur. J. Cancer*, 1992, **28A**, 1734-1742; b) H. A. Collins, M. Khurana, E. H. Moriyama, A. Mariampillai, E. Dahlstedt, M. Balaz, M. K. Kuimova, M. Drobizhev, V. X. D. Yang, D. Phillips, A. Rebane, B. C. Wilson and H. L. Anderson, *Nat. Photonics*, 2008, **2**, 420-424; c) J. R. Starkey, A. K. Rebane, M. A. Drobizhev, F. Meng, A. Gong, A. Elliott, K. McInnerney and C. W. Spangler, *Clin. Cancer Res.*, 2008, **14**, 6564-6573; d) M. Khurana, E. H. Moriyama, A. Mariampillai, K. Samkoe, D. Cramb and B. C. Wilson, *J. Biomed. Opt.*, 2009, **14**, 064006(1-14).
- a) W. Nie, *Adv. Mater.*, 1993, **5**, 520-545; b) H. S. Nalwa, *Adv. Mater.*, 1993, **5**, 341-358; c) M. G. Humphrey, T. Schwich, P. J. West, M. P. Cifuentes and M. Samoc, in *Comprehensive Inorganic Chemistry II - from Element to Applications*, eds. J. Reedijk and K. Poeppelmeier, Oxford: Elsevier, 2013, vol. 8, pp. 781-835.
- P. V. Simpson, L. A. Watson, A. Barlow, G. Wang, M. P. Cifuentes and M. G. Humphrey, *Angew. Chem. Int. Ed.*, 2016, **55**, 2387-2391
- G. Grelaud, M. P. Cifuentes, F. Paul and M. G. Humphrey, *J. Organomet. Chem.*, 2014, **751**, 181-200.
- K. A. Green, M. P. Cifuentes, M. Samoc and M. G. Humphrey, *Coord. Chem. Rev.*, 2011, **255**, 2530-2541; K. A. Green, M. P. Cifuentes, M. Samoc and M. G. Humphrey, *Coord. Chem. Rev.*, 2011, **255**, 2025-2038.
- a) T. Schwich, M. P. Cifuentes, P. A. Gugger, M. Samoc and M. G. Humphrey, *Adv. Mater.*, 2011, **23**, 1433-1435; b) M. G. Humphrey, M. P. Cifuentes and M. Samoc, *Top. Organomet. Chem.*, 2011, **28**, 57-73; c) A. Trujillo, R. Veillard, G. Argouarch, T. Roisnel, A. Singh, I. Ledoux and F. Paul, *Dalton Trans.*, 2012, **41**, 7454-7456.
- A. Triadon, G. Grelaud, N. Richey, O. Mongin, G. J. Moxey, I. M. Dixon, X. Yang, G. Wang, A. Barlow, J. Rault-Berthelot, M. P. Cifuentes, M. G. Humphrey and F. Paul, *Organometallics*, 2018, **35**, 2245-2262.
- M. Pawlicki, H. A. Collins, R. G. Denning and H. L. Anderson, *Angew. Chem. Int. Ed.*, 2009, **48**, 3244-3266.
- M. Ravikanth and K. G. Ravindra, *Curr. Sci.*, 1995, **68**, 1010-1017.
- G. de la Torre, P. Vazquez, F. Agullo-Lopez and T. Torres, *Chem. Rev.*, 2004, **104**, 3723-3750.
- S. V. Rao, N. K. M. N. Srinivas, D. N. Rao, L. Giribabu, B. G. Maiya, R. Philip and G. R. Kumar, *Optics Commun.*, 2000, **182**, 255-264.
- S. Drouet, A. Merhi, G. Grelaud, M. P. Cifuentes, M. G. Humphrey, K. Matczyszyn, M. Samoc, L. Toupet, C. O. Paul-Roth and F. Paul, *New J. Chem.*, 2012, **36**, 2192-2195.
- S. Drouet, A. Merhi, D. Yao, M. P. Cifuentes, M. G. Humphrey, M. Wielgus, J. Olesiak-Banska, K. Matczyszyn, M. Samoc, F. Paul and C. O. Paul-Roth, *Tetrahedron*, 2012, **68**, 10351-10359.
- A. Merhi, G. Grelaud, K. A. Green, H. M. Ngo, M. Reynolds, I. Ledoux, A. Barlow, G. Wang, M. P. Cifuentes, M. G. Humphrey, F. Paul and C. O. Paul-Roth, *Dalton Trans.*, 2015, **44**, 7748-7751.
- A. Merhi, G. Grelaud, N. Ripoche, A. Barlow, M. P. Cifuentes, M. G. Humphrey, F. Paul and C. O. Paul-Roth, *Polyhedron*, 2015, **86**, 64-70.
- A. Merhi, G. Grelaud, M. Morshedi, S. Abid, K. A. Green, A. Barlow, T. Groizard, S. Kahlal, J.-F. Halet, H. M. Ngo, I. Ledoux-Rak, M. P. Cifuentes, M. G. Humphrey, F. Paul and C. O. Paul-Roth, *Dalton Trans.*, 2018, **47**, 11123-11135.
- Y. Tanaka, M. Ono and M. Akita, *J. Porphyrins Phthalocyanines*, 2015, **19**, 442-450.
- a) K. Mishiba, M. Ono, Y. Tanaka and M. Akita, *Chem. Eur. J.*, 2017, **23**, 2067-2076; b) K. Onitsuka, H. Kitajima, M. Fujimoto, A. Iuchi, F. Takei and S. Takahashi, *Chem. Commun.*, 2002, 2576-2577; c) D. Bellows, S. M. Ali, C. P. Gros, M. E. Ojaimi, J.-M. Barbe, R. Guillard and P. D. Harvey, *Inorg. Chem.*, 2009, **48**, 7613-7629; d) C. Bucher, C. H. Devillers, J.-C. Moutet, G. Royal and E. Saint-Aman, *Coord. Chem. Rev.*, 2009, **253**, 21-36; e) V. N. Nemykin, G. T. Rohde, C. D. Barrett, R. G. Hadt, C. Bizzarri, P. Galloni, B. Floris, I. Nowik, R. H. Herber, A. G. Marrani, R. Zaroni and N. M. Loim, *J. Am. Chem. Soc.*, 2009, **131**, 14969-14978; f) G. T. Rohde, J. R. Sabin, C. D. Barrett and V. N. Nemykin, *New J. Chem.*, 2011, **35**, 1440-1448; g) P. Gautam, B. Dhokale, V. Shukla, C. P. Singh, K. S. Bindra and R. Misra, *J. Photochem. Photobiol. A*, 2012, **239**, 24-27; h) S. J.

- Dammer, P. V. Solntsev, J. R. Sabin and V. N. Nemykin, *Inorg. Chem.*, 2013, **52**, 9496-9510.
23. A. Merhi, X. Zhang, D. Yao, S. Drouet, O. Mongin, F. Paul, J. A. G. Williams, M. A. Fox and C. O. Paul-Roth, *Dalton Trans.*, 2015, **44**, 9470-9485.
 24. X. Zhang, S. Abid, L. Shi, J. A. G. Williams, M. A. Fox, F. Miomandre, C. Tourbillon, J.-F. Audibert, O. Mongin, F. Paul and C. O. Paul-Roth, *Dalton Trans.*, 2019, **48**, 11897-11911.
 25. a) C. O. Paul-Roth and G. Simonneaux, *Tetrahedron Lett.*, 2006, **47**, 3275-3278; C. O. Paul-Roth and G. Simonneaux, *C. R. Acad. Sci., Ser. IIB; Chim.*, 2006, **9**, 1277-1286; b) C. O. Paul-Roth, J. A. G. Williams, J. Letessier and G. Simonneaux, *Tetrahedron Lett.*, 2007, **48**, 4317-4322.
 26. M. Murai, M. Sugimoto and M. Akita, *Dalton Transactions*, 2013, **42**, 16108-16120.
 27. K. D. Bonin and T. J. McClrath, *J. Opt. Soc. Am. B* 1984, **1**, 52-55.
 28. D. Yao, X. Zhang, A. Triadon, N. Richey, O. Mongin, M. Blanchard-Desce, F. Paul and C. O. Paul-Roth, *Chem. Eur. J.*, 2017, **23**, 2635-2647.
 29. B. Li, J. Li, Y. Fu and Z. Bo, *J. Am. Chem. Soc.*, 2004, **126**, 3430-3431; B. Li, K. Xu, M. Sun, Y. Fu, G. Yu, Y. Liu and Z. Bo, *Macromolecules*, 2006, **39**, 456-461.
 30. a) T. Pei, K. Peng, X.-y. Cai, L.-j. Yuan and J.-b. Xia, *Wuli Huaxue Xuebao*, 2017, **33**, 2550-2558; b) H. Wang, F. Liu, Y. Yang, M. Zhang, C. Peng, S. Bo, X. Liu, L. Qiu and Z. Zhen, *New J. Chem.*, 2015, **39**, 1038-1044; c) D. Zhang, V. Martin, I. Garcia-Moreno, A. Costela, M. E. Perez-Ojeda and Y. Xiao, *Phys. Chem. Chem. Phys.*, 2011, **13**, 13026-13033.
 31. H. Su, S. Zhu, M. Qu, R. Liu, G. Song and H. Zhu, *J. Phys. Chem. C*, 2019, **123**, 15685-15692.
 32. D. Yao, X. Zhang, S. Abid and C. O. Paul-Roth, *J. Photochem. Photobiol. A*, 2017, **338**, 96-103.
 33. a) J. S. Lindsey, K. A. Maccrum, J. S. Tychonas and Y. Y. Chuang, *J. Org. Chem.*, 1994, **59**, 579-587; b) F. R. Li, K. X. Yang, J. S. Tychonas, K. A. Maccrum and J. S. Lindsey, *Tetrahedron*, 1997, **53**, 12339-12360.
 34. X. Zhang, S. Ben Hassine, N. Richey, O. Mongin, M. Blanchard-Desce, F. Paul and C. O. Paul-Roth, *New J. Chem.*, 2020, **44**, 4144-4157.
 35. N. Gauthier, C. Olivier, S. Rigaut, D. Touchard, T. Roisnel, M. G. Humphrey and F. Paul, *Organometallics*, 2008, **27**, 1063-1072.
 36. F. Malvolti, C. Rouxel, G. Grelaud, L. Toupet, T. Roisnel, X. Yang, G. Wang, A. Barlow, F. I. Abdul Razak, R. Stranger, M. P. Cifuentes, M. G. Humphrey, O. Mongin, M. Blanchard-Desce, C. O. Paul-Roth and F. Paul, *Eur. J. Inorg. Chem.*, 2016, 3868-3882.
 37. N. G. Connelly and W. E. Geiger, *Chem. Rev.*, 1996, **96**, 877-910.
 38. a) M. I. Bruce, A. Burgun, M. A. Fox, M. Jevric, P. J. Low, B. K. Nicholson, C. R. Parker, B. W. Skelton, A. H. White and N. N. Zaitseva, *Organometallics*, 2013, **32**, 3286-3299; b) M. I. Bruce, M. A. Fox, P. J. Low, B. K. Nicholson, C. R. Parker, W. C. Patalinghug, B. W. Skelton and A. H. White, *Organometallics*, 2012, **31**, 2639-2657; c) M. A. Fox, R. L. Roberts, T. E. Baines, B. Le Guennic, J.-F. Halet, F. Hartl, D. S. Yufit, D. Albesa-Jove, J. A. K. Howard and P. J. Low, *J. Am. Chem. Soc.*, 2008, **130**, 3566-3578; d) M. A. Fox, R. L. Roberts, W. M. Khairul, F. Hartl and P. J. Low, *J. Organomet. Chem.*, 2007, **692**, 3277-3290; e) M. A. Fox, B. Le Guennic, R. L. Roberts, D. A. Brue, D. S. Yufit, J. A. K. Howard, G. Manca, J.-F. Halet, F. Hartl and P. J. Low, *J. Am. Chem. Soc.*, 2011, **133**, 18433-18446; f) M. C. Walkey, L. T. Byrne, M. J. Piggott, P. J. Low and G. A. Koutsantonis, *Dalton Trans.*, 2015, **44**, 8812-8815.
 39. M. Kasha, H. R. Rawls and A. El-Bayoumi, *Pure & Appl. Chem.*, 1965, **11**, 371-392.
 40. a) M. Calvete, G. Y. Yang and M. Hanack, *Synth. Met.*, 2004, **141**, 231-243; b) F. Z. Henari, *J. Opt. A: Pure Appl. Opt.*, 2001, **3**, 188-190; c) K. J. McEwan, G. Bourhill, J. M. Robertson and H. L. Anderson, *J. Nonlinear Opt. Phys. & Mat.*, 2000, **9**, 451-468.
 41. M. G. Kuzyk, *J. Chem. Phys.*, 2003, **119**, 8327-8334.
 42. M. G. Kuzyk, *J. Mater. Chem.*, 2009, **19**, 7444-7465.
 43. G. Boudebs, C. Cassagne, H. Wang, J.-L. Godet and C. B. de Araújo, *J. Luminescence*, 2018, **199**, 319-322.
 44. F. Bolze, S. Jenni, A. Sour and V. Heitz, *Chem. Commun.*, 2017, **53**, 12857-12877.
 45. X. Zhou, A.-M. Ren, J.-K. Feng, X.-J. Liu and Y.-D. Zhang, *Chem. Phys. Chem.*, 2004, **4**, 991-997.
 46. R. L. Roberts, T. Schwich, T. C. Corkery, M. P. Cifuentes, K. A. Green, J. D. Farmer, P. J. Low, T. B. Marder, M. Samoc and M. G. Humphrey, *Adv. Mater.*, 2009, **21**, 2318-2322.
 47. C. W. Spangler, *J. Mater. Chem.*, 1999, **9**, 2013-2020.
 48. D. D. Perrin and W. L. F. Armarego, *Purification of Laboratory Chemicals*, Pergamon Press, Oxford, 3rd ed., 1988.
 49. M. A. Fox, J. E. Harris, S. Heider, V. Pérez-Gregorio, M. E. Zakrzewska, J. D. Farmer, D. S. Yufit, J. A. K. Howard and P. J. Low, *J. Organomet. Chem.*, 2009, **694**, 2350-2358.
 50. J. R. Polam and L. C. Porter, *J. Coord. Chem.*, 1993, **29**, 109-119.
 51. M. J. Frisch, G. W. Trucks, H. B. Schlegel, G. E. Scuseria, M. A. Robb, J. R. Cheeseman, G. Scalmani, V. Barone, B. Mennucci, G. A. Petersson, H. Nakatsuji, M. Caricato, X. Li, H. P. Hratchian, A. F. Izmaylov, J. Bloino, G. Zheng, J. L. Sonnenberg, M. Hada, M. Ehara, K. Toyota, R. Fukuda, J. Hasegawa, M. Ishida, T. Nakajima, Y. Honda, O. Kitao, H. Nakai, J. T. Vreven, J. A. Montgomery, J. E. Peralta, F. Ogliaro, M. Bearpark, J. J. Heyd, E. Brothers, K. N. Kudin, V. N. Staroverov, R. Kobayashi, J. Normand, K. Raghavachari, A. Rendell, J. C. Burant, S. S. Iyengar, J. Tomasi, M. Cossi, N. Rega, J. M. Millam, M. Klene, J. E. Knox, J. B. Cross, V. Bakken, C. Adamo, J. Jaramillo, R. Gomperts, R. E. Stratmann, O. Yazyev, A. J. Austin, R. Cammi, C. Pomelli, J. W. Ochterski, R. L. Martin, K. Morokuma, V. G. Zakrzewski, G. A. Voth, P. Salvador, J. J. Dannenberg, S. Dapprich, A. D. Daniels, O. Farkas, J. B. Foresman, J. V. Ortiz, J. Cioslowski and D. J. Fox, *Journal*, 2009.
 52. a) A. D. Becke, *J. Chem. Phys.*, 1993, **98**, 5648-5652; b) C. Lee, W. Yang and R. G. Parr, *Phys. Rev. B*, 1988, **37**, 785-789.
 53. a) G. A. Petersson, A. Bennett, T. G. Tensfeldt, M. A. Al-Laham, W. A. Shirley and J. Mantzaris, *J. Chem. Phys.*, 1988, **89**, 2193-2218; b) G. A. Petersson and M. A. Al-Laham, *J. Chem. Phys.*, 1991, **94**, 6081-6090.
 54. A.-R. Allouche, *J. Comput. Chem.*, 2011, **32**, 174-182.
 55. N. M. O'Boyle, A. L. Tenderholt and K. M. Langner, *J. Comp. Chem.*, 2008, **29**, 839-845.

